ACS OMEGA

http://pubs.acs.org/journal/acsodf

Article

^{89}Zr-DFO-Isatuximab for CD38-Targeted ImmunoPET Imaging of Multiple Myeloma and Lymphomas

Natalia Herrero Alvarez, Alexa L. Michel, Tara D. Viray, Marius E. Mayerhoefer, and Jason S. Lewis*

Cite This: *ACS Omega* 2023, 8, 22486−22495

Read Online

ACCESS | Metrics & More | Article Recommendations | Supporting Information

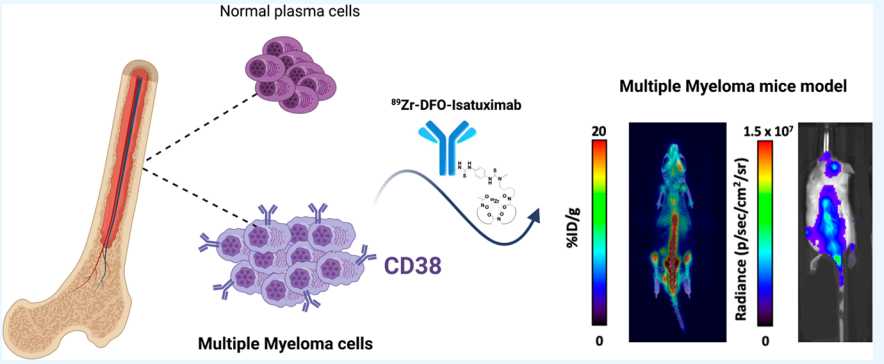

ABSTRACT: Multiple myeloma (MM) is the second most prevalent hematological malignancy. It remains incurable despite the availability of novel therapeutic approaches, marking an urgent need for new agents for noninvasive targeted imaging of MM lesions. CD38 has proven to be an excellent biomarker due to its high expression in aberrant lymphoid and myeloid cells relative to normal cell populations. Using isatuximab (Sanofi), the latest FDA-approved CD38-targeting antibody, we have developed Zirconium-89(^{89}Zr)-labeled isatuximab as a novel immunoPET tracer for the *in vivo* delineation of MM and evaluated the extension of its applicability to lymphomas. *In vitro* studies validated the high binding affinity and specificity of ^{89}Zr-DFO-isatuximab for CD38. PET imaging demonstrated the high performance of ^{89}Zr-DFO-isatuximab as a targeted imaging agent to delineate tumor burden in disseminated models of MM and Burkitt's lymphoma. *Ex vivo* biodistribution studies confirmed that high accumulations of the tracer in bone marrow and bone skeleton correspond to specific disease lesions as they are reduced to background in blocking and healthy controls. This work demonstrates the promise of ^{89}Zr-DFO-isatuximab as an immunoPET tracer for CD38-targeted imaging of MM and certain lymphomas. More importantly, its potential as an alternative to ^{89}Zr-DFO-daratumumab holds great clinical relevance.

INTRODUCTION

Multiple myeloma (MM) represents the second most common hematological malignancy, accounting for 2% of all cancers and 19% of hematological tumors.[1] While novel therapeutic approaches and new treatments have been successfully introduced in recent years, improving the prognosis and therapy of MM will depend on the accurate measurement of disease burden: MM remains incurable largely due to suboptimal means of measuring disease burden.[2] Only sensitive detection of disease burden allows for early intervention, which is directly associated with progression-free and overall survival. Furthermore, detection of minimal residual disease (MRD) following therapy is crucial to improving the prognosis of MM patients, as most eventually relapse. Thus, a sensitive method of detecting and measuring tumor burden is urgently needed.[3]

The ability to assess the expression levels of selected targets in MM cells before and during treatment will also help to stratify patients according to their likelihood of responding to the corresponding therapy, in part by helping to identify dynamic expression that has been downregulated and thus contribute to disease resistance.[4] Likewise, baseline evaluation of and differentiation between active and inactive lesions after therapy is essential to evaluating therapeutic efficacy and better managing clinical decision-making. In this context, imaging plays a pivotal role in the management of the malignancy. More specifically, PET has proven to be a powerful molecular imaging tool for these unmet clinical needs, targeting different molecular pathways and facilitating the development of promising tracers.[5]

Among the new generation of therapeutic targets, CD38, or cluster of differentiation 38, has attracted great attention in recent years due to its high expression in aberrant lymphoid

Received: January 30, 2023
Accepted: March 30, 2023
Published: April 11, 2023

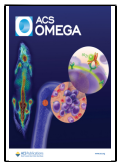

and myeloid cells relative to normal cell populations. CD38 is a 45-kD, type II transmembrane glycoprotein that metabolizes NAD^+, regulates cytoplasmic Ca^{2+} flux, and mediates signal transduction.[6] Its expression is induced by inflammatory cytokines, endotoxins, interferons, and some nuclear receptors. Thus, an extensive range of (radio)pharmaceuticals have been designed to target and/or modulate its activity, some of which have already shown some success in early clinical trials in plasma cell malignancies.[7] This makes CD38 an excellent biomarker for targeted imaging and therapy in MM.[8]

Certainly, anti-CD38 monoclonal antibodies have already shown high efficiency in the immunotherapy of MM, and preclinical studies highlight their potential use in other CD38-positive hematologic malignancies, including lymphomas and leukemias.[9] Daratumumab (Janssen Pharmaceuticals) was the first CD38-targeting antibody approved by the FDA as a single agent in MM immunotherapy treatment.[10] Labeling of the native daratumumab with positron-emitting radionuclides such as zirconium-89 has been exploited for immunoPET imaging in different models of disease, proving particularly successful in MM.[11] Our group previously reported the synthesis of ^{89}Zr-DFO-daratumumab for CD38-targeted immunologic PET imaging of MM in a murine model and a successful first-in-human imaging study.[12] ^{89}Zr-DFO-daratumumab demonstrated successful uptake in osseous deposits in patients with MM and the ability to image myeloma that was not detected by 18F-FDG, the current standard-of-care imaging. Daratumumab has also been labeled with therapeutic nuclides, demonstrating the validity for CD38-targeted radioimmunotherapy in different preclinical models.[13,14] Finally, extension to other targeted molecular imaging modalities has been explored by conjugation to different dyes.[15]

However, despite these promising results, daratumumab resistance, which occurs in approximately 60% of patients, is a recurrent problem hampering clinical response.[9,16,17] The underlying mechanisms of resistance include clone selection of $CD38^{dim}$ myeloma cells;[9] CD38 reduction, for instance by CD38 endocytosis/internalization;[18] immunomodulation, for instance by downregulation of intracellular pathways in bone marrow stem/stromal cells and a decrease of effector memory T cells and M1 macrophages;[19,20] and prevention of complement-dependent cytotoxicity, for instance via CD55 and CD59 overexpression.[21]

Isatuximab (Sanofi), the latest CD38-targeting antibody approved by the FDA (March 2021) for MM treatment, has shown encouraging results. In a phase 1b trial, combination of isatuximab with pomalidomide and dexamethasone showed an overall response rate of 53.2% in 47 MM patients, 14.9% of which were refractory to daratumumab.[22] In a multicentric phase 1/2 study in relapsed/refractory MM patients who had demonstrated disease progression under daratumumab mono- or combination therapy, isatuximab monotherapy enabled a ≥8-week disease control rate (stable disease or minor response) of 37.5%.[23]

While belonging to the same IgG1-κ subclass and targeting the same receptor, very distinct mechanisms of action and binding modes have been reported between daratumumab and isatuximab, including the identification of their corresponding binding epitopes.[24−26] These structural and functional features have very important implications for the rational design of targeted pharmaceuticals,[27] sparking investigations into the possibility that isatuximab could overcome daratumumab resistance.[28] In this context, development of isatuximab as an imaging agent would expand the means to detect and quantify CD38-positive tumors and might potentially help elucidate these mechanisms of action and resistance, whether primary or acquired. A better understanding of the immune effector mechanism of each antibody is necessary to better predict patient response and treatment monitoring.[29] Additionally, some treatment features that greatly impact patient quality of life, such as administration route and regimes, have been reported as more favorable for isatuximab than daratumumab.[30] Accordingly, validation of isatuximab as an imaging and potentially therapeutic agent would have a high translational relevance for those patients who could benefit from this new mAb in the era of personalized medicine.[31]

Here, we present the radiolabeling of the native isatuximab with the PET emitter radionuclide ^{89}Zr and the preclinical evaluation of its potency as an immunoPET tracer for CD38-targeted imaging. In this study, we detail the synthesis and the *in vitro* and *in vivo* comparison to ^{89}Zr-DFO-daratumumab in MM and lymphoma murine models.

MATERIALS AND METHODS

Cell Culture. All cell lines were obtained from the American Type Culture Collection (ATCC). Cultures were grown in aseptic conditions at 37 °C and 5% CO_2 in a humidified atmosphere in RPMI-1640 medium supplemented with 10% fetal bovine serum, 2 mM L-glutamine, 100 units/mL penicillin, and 100 μg/mL streptomycin. MM.1S and Daudi cells were stably transfected with firefly luciferase (Luc) through a lentivirus, allowing for bioluminescence imaging (BLI). Successful transfection was confirmed by a luciferase reporter assay (Promega).

Flow Cytometry. The surface expression level of the CD38 receptor was evaluated and quantified before and after luciferase transfection by flow cytometry. Cells (5×10^5 cells) were incubated with FcR human blocking reagent (Milteny Biotech) in 50 μL of flow cytometry staining buffer (Invitrogen) for 15 min and subsequently stained with phycoerythrin (PE)-conjugated antihuman CD38 antibody (Biolegend clone HB-7) for 30 min. Dead cells were excluded using 4′,6-diamidine-2′-phenylindole dihydrochloride (DAPI) (Sigma-Aldrich). Cells were analyzed on a Fortessa flow cytometer, and data was processed with FlowJo V10 (treeStar). Gating of CD38 positive cells was performed using unstained controls.

Conjugation and Radiolabeling. Isatuximab (Sarclisa) and daratumumab (Darzalex) were conjugated to the chelator *p*-isothiocyanatobenzoyl desferrioxamine (*p*-SCN-DFO, Macrocyclics, Inc.) The antibodies were prepared as a 2 mg/mL solution in PBS, and the solution pH was adjusted to 9 with 0.1 M Na_2CO_3. DFO-NCS was dissolved in dry DMSO at a concentration of 10 mg/mL, and a 4-fold molar excess was added to the corresponding solutions. The reaction was incubated at 37 °C for 1 h on a thermomixer. Purification of the immunoconjugates was performed with a prepacked disposable PD-10 desalting column (GE Healthcare) and concentrated with a 50,000 MWCO Amicon centrifugal filter (Millipore Sigma). Final concentrations were determined with a NanoDrop 2000 spectrometer (Thermo Fisher Scientific). Zirconium-89 (^{89}Zr) was supplied by 3D Imaging LLC (Little Rock, AR) in 0.1 M oxalic acid. After adjusting the pH of the solution to 7 with 0.1 M $NaHCO_3$, each DFO-conjugated antibody was added to the neutralized ^{89}Zr and reacted at 37 °C for 1 h. Radiochemical purity (RCP) was assessed by radio-

https://doi.org/10.1021/acsomega.3c00624
ACS Omega 2023, 8, 22486−22495

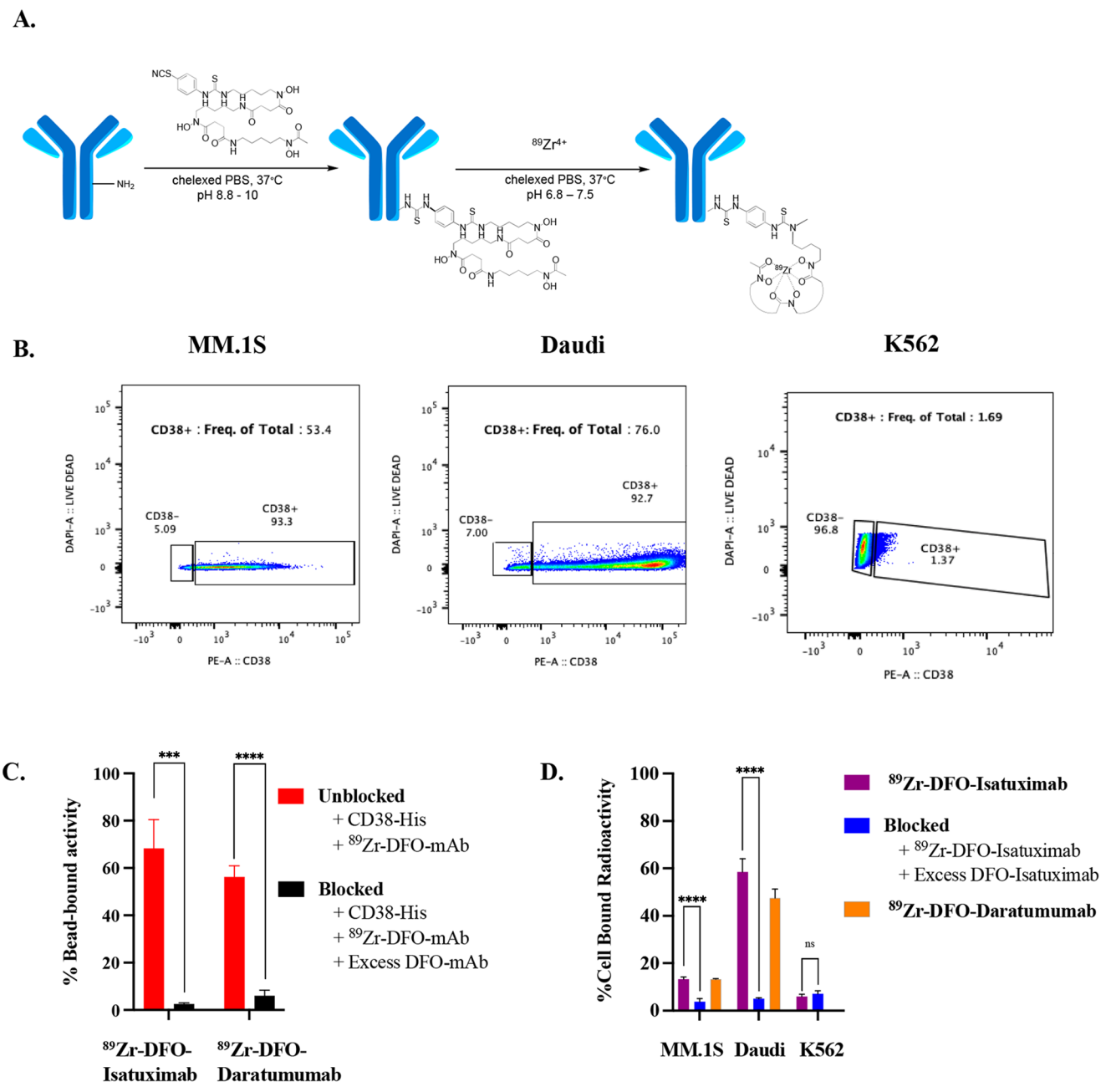

Figure 1. Synthesis of ^{89}Zr-DFO-isatuximab and validation of its potential as a CD38-targeting imaging agent. (A.) Schematic representation of ^{89}Zr-DFO-isatuximab preparation by DFO conjugation and subsequent ^{89}Zr-radiolabeling. (B) Flow cytometry quantification of CD38 receptor expression in MM.1S, Daudi, and K562 cells. (C) ^{89}Zr-DFO-isatuximab displays high and specific binding to human CD38-coupled magnetic beads. Binding is completely blocked in the presence of 1000-fold excess of unlabeled DFO-isatuximab. Parallel assessment of ^{89}Zr-DFO-daratumumab using the same assay is shown. (D) Cell binding assay confirms ^{89}Zr-DFO-isatuximab targets the CD38 surface receptor on MM MM.1S cells and Burkitt's lymphoma Daudi cells. The cell line K562 is used as a CD38− control. Specificity of binding is shown in the presence of 25-fold excess of unlabeled DFO-isatuximab. Parallel assessment of ^{89}Zr-DFO-daratumumab using the same assay is shown for the CD38+ lines. ns $p > 0.05$, ***$p < 0.0005$, ****$p < 0.0001$.

instant thin-layer chromatography (radio-iTLC) using 50 mM ethylenediaminetetraacetic acid (EDTA) as the eluent and was always greater than 99% before injection.

Binding Studies. Cell binding assays were performed by incubating the different cell lines with 1 μCi of ^{89}Zr-DFO-mAb in PBS with 1% BSA for 2 h at 4 °C. Excess of unlabeled DFO-mAb was added in the blocking group to demonstrate the specificity of the binding. Unbound radiotracer was removed by washing the cells twice with ice-cold PBS and centrifuging (600*g* for 5 min). The radioactivity of the different fractions was measured using a gamma counter.

Animals and Tumor Models. All animal experiments performed in this study were approved by the Institutional Animal Care and Use Committee and Research Animal Resource Center at Memorial Sloan Kettering Cancer Center. *In vivo* imaging and tissue biodistribution studies were performed in female NSG mice (NOD.Cg-*Prkdcscid Il2rgtm1Wjl*/SzJ; 6−8 weeks old; Jackson Laboratories, Bar

https://doi.org/10.1021/acsomega.3c00624
ACS Omega 2023, 8, 22486−22495

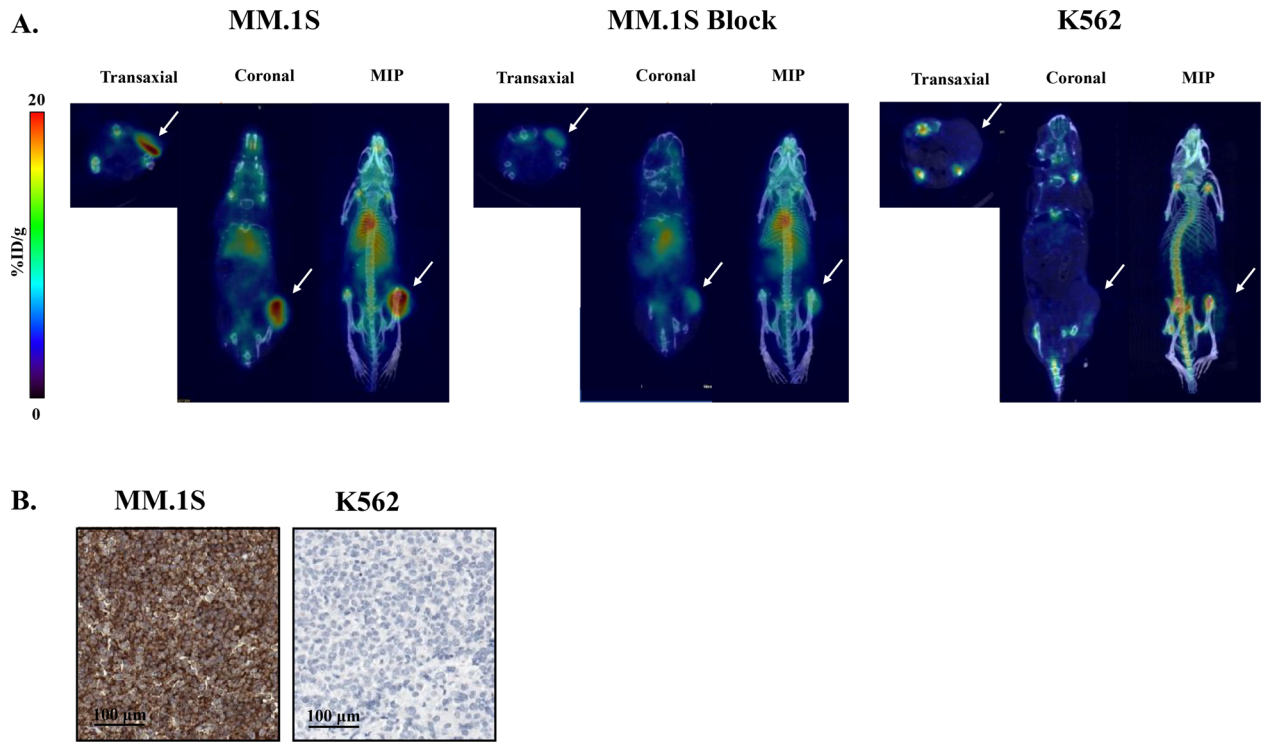

Figure 2. *In vivo* evaluation of ^{89}Zr-DFO-isatuximab in a subcutaneous model of multiple myeloma. (A) PET/CT and MIP images of ^{89}Zr-DFO-isatuximab in subcutaneous xenografts at 144 h postinjection. Tumor is located on the right flank and marked with a white arrow. *In vivo* imaging validates ^{89}Zr-DFO-isatuximab as a specific CD38-targeting agent. Decrease of tumor uptake (26 ± 4.1 vs 14.1 ± 1.7%ID/g) effected by the blocking dose (12-fold excess of unlabeled DFO-isatuximab) demonstrates specificity of the binding. Additionally, no tumor uptake is further confirmed in the negative control K562 xenograft model. (B) Representative immunohistochemistry images of MM.1S (left) and K562 (right) tumor cell selection. Scale bars, 100 μm.

Harbor, Maine). MM.1S and K562 cells (5×10^6 cells) were subcutaneously (SQ) injected in a 1:1 mixture of culture medium and Matrigel into the right flank to establish the SQ model. MM.1S-Luc and Daudi-Luc cells (1×10^6 cells) were intravenously injected in the tail vein for the disseminated model of disease. Solid SQ tumors were regularly measured with a caliper. Disseminated tumor burden was monitored by BLI. Mice were injected with 100 μL of 15 mg/mL luciferin 10 min prior to imaging with an IVIS SpectrumCT (PerkinElmer, Melville, NY).

ImmunoPET/CT Imaging Studies and Analysis. For PET imaging studies, tumor-bearing mice were intravenously injected with ^{89}Zr-DFO-isatuximab or ^{89}Zr-DFO-daratumumab (n = 4/group) (5−7.5 MBq; 18.7−25 μg). For blocking studies (n = 4) blocked mice were co-injected with a 12-fold excess of unlabeled DFO-isatuximab to block relevant receptors and demonstrate specific binding of the tracer to CD38. An additional control group of healthy mice (n = 3) was also included in the experiment. To avoid anomalous biodistribution caused by the lack of endogenous immunoglobulin G in NSG mice, 500 μg of nonspecific human immunoglobulin G was either coinjected with the radiolabeled antibody or, in the case of the blocking study, injected 3 days before the radiotracer. *In vivo* small animal PET/CT was performed on an Inveon micro PET/CT instrument (Siemens, Erlangen, Germany). Mice were anesthetized with 1−2% isoflurane, and static images were collected for a maximum of 45 min. Images were analyzed using the Inveon Research Workstation (IRW) software.

***Ex Vivo* Biodistribution Studies.** Biodistribution studies were performed by euthanizing five mice at discrete time points after injection of the tracer (0.37−1.1 MBq; 2.0−2.5 μg). Acute biodistribution of the imaging groups (5−7.5 MBq; 18.7−25 μg) was performed at the terminal time point of the corresponding study (144 h). Relevant organs including bone marrow were harvested and weighed, and radioactivity was counted on an automated gamma counter (PerkinElmer). Bone marrow was extracted by dissecting out both mouse hind limbs and centrifuging the femurs and tibias. Biodistribution values are presented as the percent of the injected dose per gram (%ID/g), determined by counting relevant standards along with organ samples and normalizing the counts per sample to the total amount of activity injected.

Autoradiography Imaging. Autoradiography was performed on frozen bone sections. Femurs, tibias, and hips were sliced in sections of 300−500 μm, using a Vantik Qs11 Cryostat, and exposed to the same phosphor screen for 24 h. The film was read on Typhoon FLA 7000 (GE Healthcare) and produced images analyzed with ImageJ software.

***Ex vivo* Flow Cytometry.** *Ex vivo* flow cytometry of the bone marrow was performed to quantify CD38 expression. Bone marrow was obtained from the femurs using a centrifugation protocol.

Tissue Immunohistochemistry Staining. The immunohistochemistry detection of CD38 was performed at Molecular Cytology Core Facility of Memorial Sloan Kettering Cancer Center, using a Discovery XT processor (Ventana Medical Systems, Roche, AZ). Femurs were decalcified prior to sectioning.

https://doi.org/10.1021/acsomega.3c00624
ACS Omega 2023, 8, 22486−22495

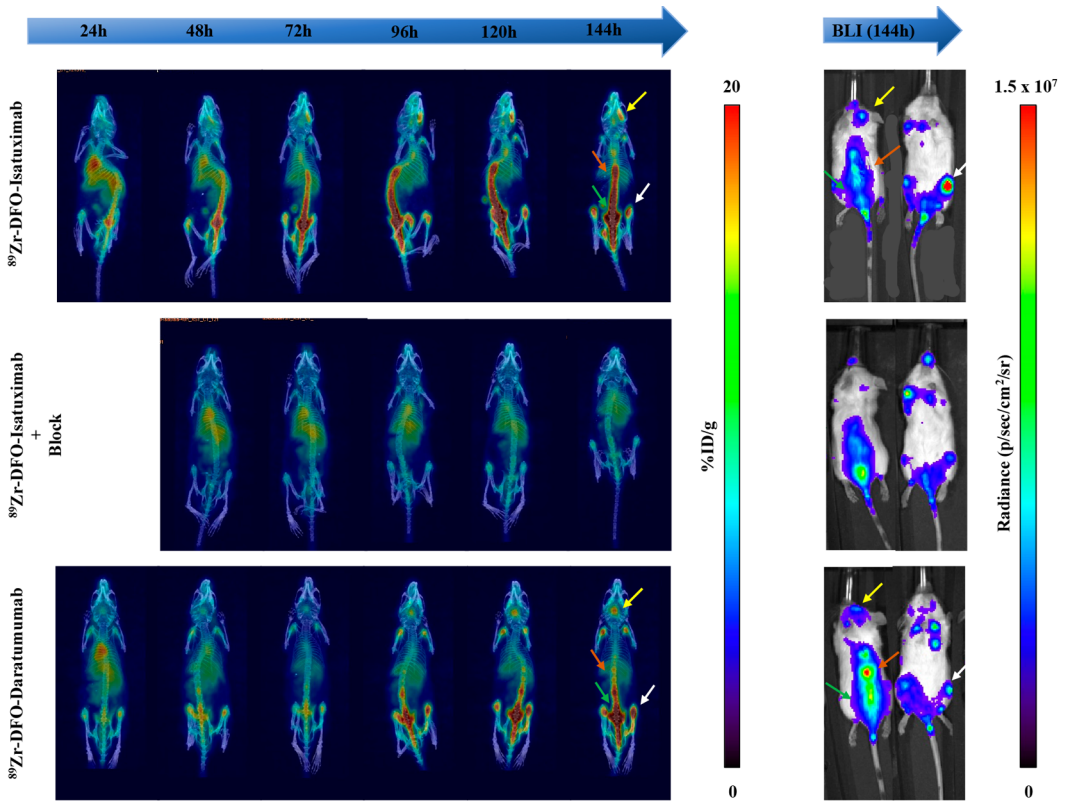

Figure 3. *In vivo* evaluation of ^{89}Zr-DFO-isatuximab in a disseminated model of multiple myeloma. MIP images at 24 h intervals up to 144 h after administration of ^{89}Zr-DFO-isatuximab in control and block cohort. Uptake pattern of the tracer matches the cancer location, as demonstrated by BLI. White arrows indicate knees, green arrows indicate pelvis, red arrows indicate lumbar spine, and yellow arrows indicate scalp. Images show ^{89}Zr-DFO-isatuximab has a high uptake in the tumor lesions, producing an excellent contrast. The block cohort exhibits no specific tumor uptake. Parallel assessment of ^{89}Zr-DFO-daratumumab in the same model of disease is shown.

Statistical Analysis. All data presented are expressed as mean ± SD. To evaluate the blocking and healthy cohort, a 2-way ANOVA test using GraphPad Prism 9 software was performed with a threshold for statistical significance set at $p < 0.05$. A correction for multiple comparisons was performed using the Holm−Sidak method to determine statistical significance ($\alpha = 0.05$). Automated image processing and automated analysis were used where possible to eliminate human bias.

RESULTS

^{89}Zr-DFO-Isatuximab Synthesis and *In Vitro* Assessment of CD38 Targeting. Development of ^{89}Zr-DFO-isatuximab as an immunoPET agent was achieved by incorporation of the PET radioisotope (Figure 1A). Chemical modification of the native commercial antibody by covalent conjugation of the chelator DFO on nonsite specific lysine residues allowed the radiolabeling with ^{89}Zr. Synthesis of ^{89}Zr-DFO-isatuximab was successfully accomplished with yields higher than 92% ($n = 10$). Purified radioimmunoconjugate had a radiochemical purity greater than 99%, with no detectable free ^{89}Zr, and specific activities of 33.3 ± 3.7 MBq/mg. Additionally, ^{89}Zr-DFO-isatuximab exhibited an excellent *in vitro* stability, displaying >90% in PBS and human serum over 144 h (Figure S1). The same methodology was followed for the synthesis of ^{89}Zr-DFO-daratumumab.

Binding of the new radioimmunoconjugate to the target was first validated in a magnetic bead assay.[32] ^{89}Zr-DFO-isatuximab exhibited successful binding to CD38, comparable to that of ^{89}Zr-DFO-daratumumab, and was blockable in the presence of a 1000-fold excess of unlabeled DFO-isatuximab (Figure 1C).

For cellular studies, human MM, MM.1S cell line, Burkitt's lymphoma, Daudi cell line, and myelogenous leukemia, K562 cell line, were used. Cellular expression of CD38 receptor for the three lines was validated by flow cytometry (Figure 1B). *In vitro* cell assays confirmed that ^{89}Zr-DFO-isatuximab binds to the cell surface receptor on the CD38+ cell lines and displays a better performance on Daudi cells, which is in accordance with the higher density of CD38 in this cell line. Binding remained baseline and non-blockable on the CD38− cell line (Figure 1D).

***In Vivo* Evaluation of ^{89}Zr-DFO-isatuximab in Subcutaneous Xenograft Models.** After *in vitro* validation of its CD38-targeting potential, we evaluated the imaging performance of ^{89}Zr-DFO-isatuximab in a subcutaneous xenograft model of human MM. PET/CT and maximum-intensity-projection images (MIP) with ^{89}Zr-DFO-isatuximab showed a high delineation of the tumor at 144 h after injection of the tracer (Figure 2A). For the blocking group, tumor uptake was significantly reduced in comparison with the control (26 ± 4.1% vs 14.1 ± 1.7%ID/g), which proved the specificity of the tracer for the CD38 receptor. A subcutaneous xenograft of K562, which does not express CD38, was used as a negative model. Immunohistochemistry analysis of resected MM.1S and K562 tumors confirmed expression or lack of CD38, respectively (Figures 2B and S2).

https://doi.org/10.1021/acsomega.3c00624
ACS Omega 2023, 8, 22486−22495

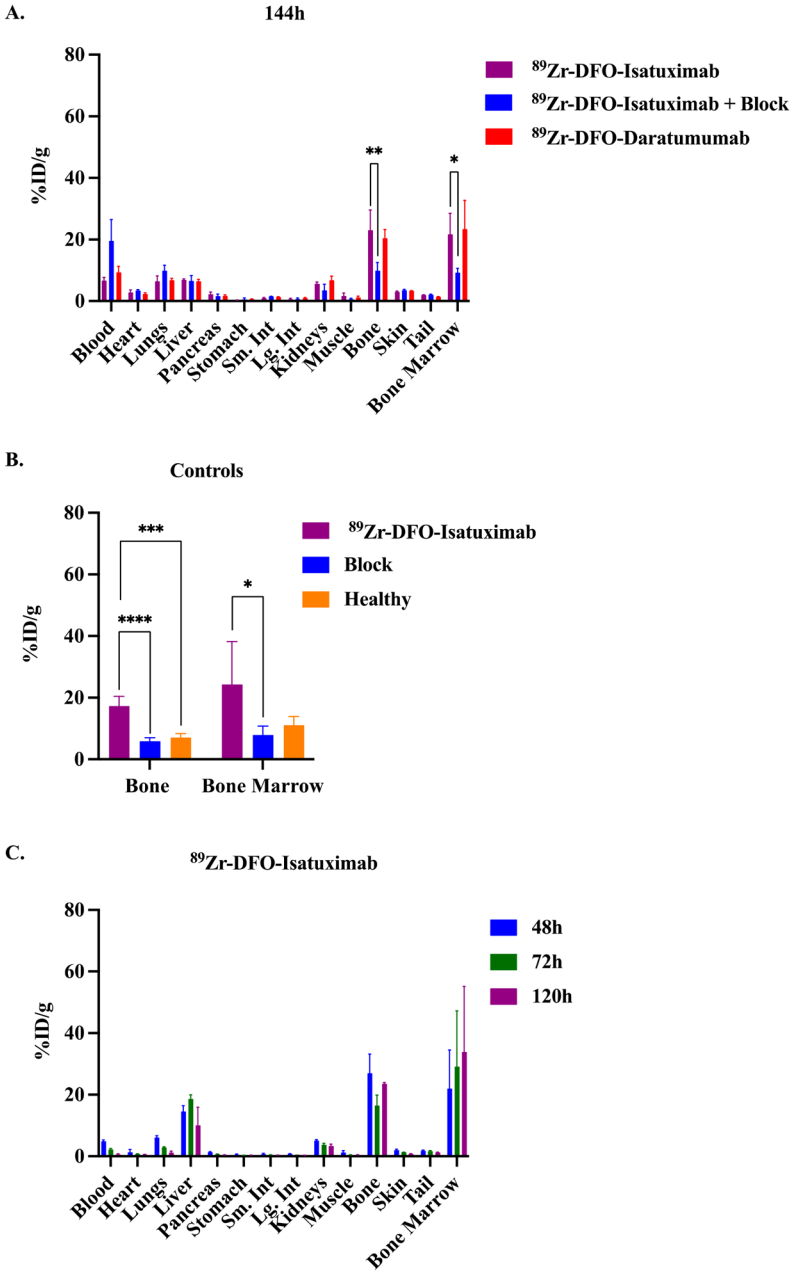

Figure 4. Biodistribution studies of ^{89}Zr-DFO-isatuximab in a disseminated model of multiple myeloma. (A) Terminal point biodistribution in the MM1.S disseminated model imaging group, at 144 h after administration of the radiotracer. Block cohort and ^{89}Zr-DFO-daratumumab evaluations are included. (B) Control *ex vivo* biodistribution of ^{89}Zr-DFO-isatuximab. Radiotracer uptake in bone and bone marrow is shown for MM.1S-Luc-injected mice, block cohort, and healthy NSG mice at 144 h after administration. (C) Time-course *ex vivo* biodistribution of ^{89}Zr-DFO-isatuximab in a MM1.S disseminated model indicating relatively slow clearance from blood and lungs, relatively constant liver uptake, and increasing specific uptake in bone and bone marrow. All data are shown as mean ± SD.

CD38-Targeted PET Imaging of ^{89}Zr-DFO-Isatuximab in a Disseminated Murine Model of Multiple Myeloma. We aimed to evaluate ^{89}Zr-DFO-isatuximab in a disseminated model of disease which is more consistent with the real pathology of hematological malignancies. A disseminated MM model was generated by intravenous injection of MM1.S-Luc cells into NSG mice. Mice were monitored by BLI. After photon flux reached an average of 1×10^7 p/sec/cm^2/sr, approximately 3−4 weeks after cell injection, they were randomized into the different groups. Diseased mice received ^{89}Zr-DFO-isatuximab, ^{89}Zr-DFO-isatuximab coinjected with a blocking dose of DFO-isatuximab, and ^{89}Zr-DFO-daratumumab, respectively. Additionally, ^{89}Zr-DFO-isatuximab was administered to a group of healthy NSG mice. Mice were imaged at 24, 48, 72, 96, 120 and 144 h upon tracer injection (Figure 3). A complete biodistribution study was performed at the last time point (144 h) to quantify the radiotracer uptake in major organs for each cohort (Figure 4A and Table S1). Bone marrow was extracted from the femurs by centrifugation and counted separately from the bone (femur or tibia), which was measured unprocessed. %ID/g values confirmed high uptake of ^{89}Zr-DFO-isatuximab in bone and bone marrow (23.0 ± 6.5% and 21.7 ± 6.8%ID/g, respectively), which was

https://doi.org/10.1021/acsomega.3c00624
ACS Omega 2023, 8, 22486−22495

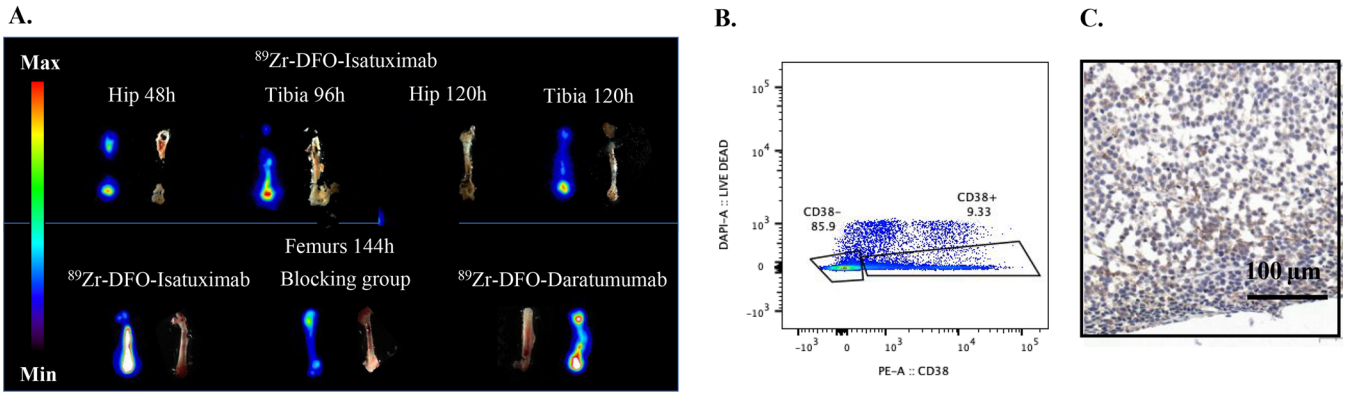

Figure 5. *Ex vivo* autoradiography, flow cytometry, and IHC analysis. (A) Autoradiography and overlapping microscope imaging indicating uptake of ^{89}Zr-DFO-isatuximab by hips and tibias at different postinjection times (top), and uptake comparison of ^{89}Zr-DFO-isatuximab in blocking and normal cohort with ^{89}Zr-DFO-daratumumab by femurs at 144 h (bottom). All sections were exposed to the same phosphor imaging screen and incubated together. (B) *Ex vivo* flow cytometry analysis of bone marrow cells in MM.1S-injected mice for CD38 receptor expression quantification. (C) Representative immunohistochemistry images of MM1.S disseminated model. Femur sections stained for CD38. Scale bars, 100 μm.

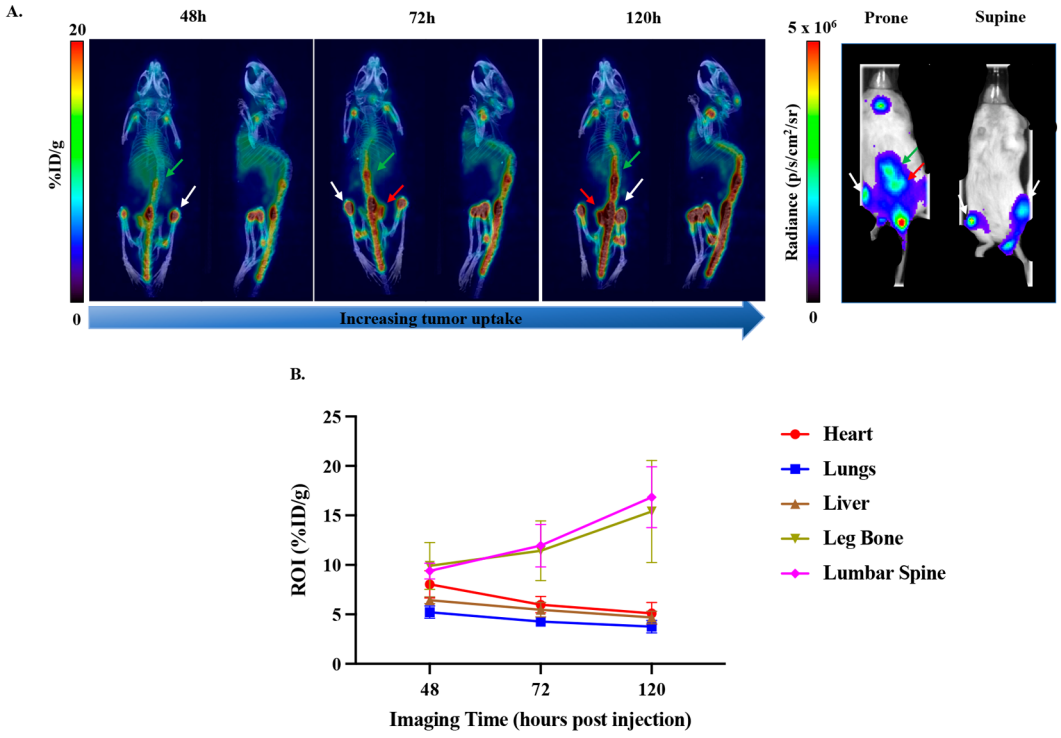

Figure 6. *In vivo* evaluation of^{89}Zr-DFO-isatuximab in a disseminated model of Burkitt's lymphoma. (A) Representative time-course MIP images at 48, 72, and 120 h after administration of ^{89}Zr-DFO-isatuximab in Daudi-Luc-injected mice. Uptake of ^{89}Zr-DFO-isatuximab clearly increases over time, displaying an excellent delineation of the lesions. The pattern of the tracer matches the cancer location, as demonstrated by the bioluminescence imaging. White arrows indicate knees, red arrows indicate pelvis, and green arrows indicate lumbar spine. Bioluminescence imaging demonstrates the location of cancer cells in the disease model. Images were taken no more than 24 h before administration of radiotracer. (B) Semiquantitative analysis of ^{89}Zr-DFO-isatuximab uptake in a disseminated Daudi model over a 5-day time course. ROI were drawn on transaxial PET images at the location corresponding to the anatomic location of the selected organs. Time−activity curves indicate slow clearance of the radiotracer from heart (blood pool), liver, and lungs; a relatively constant uptake in bone; and increasing uptake in the lumbar spine.

statistically significant compared to the uptake in the blocking group (9.8 ± 2.6%ID/g; $P < 0.0005$ and 9.2 ± 1.3%ID/g; $P < 0.05$, respectively), and as good as uptake with ^{89}Zr-DFO-daratumumab (20.4 ± 2.7% and 23.4 ± 9.3%ID/g). Additionally, a control experiment was conducted to compare the uptake of ^{89}Zr-DFO-isatuximab in bone and bone marrow between diseased mice, a blocking group, and a healthy cohort (Figure 4B). This study revealed a minimal amount of tracer accumulation in bone and marrow (6.7 ± 0.6%ID/g; $P < 0.0005$, 11.1 ± 2.7%ID/g; $P < 0.05$), one of the main concerns when working with ^{89}Zr-mAbs, which increases background-to-tumor signal.

***Ex Vivo* Biodistribution Study.** The time-course biodistributon study (Figure 4C) confirmed the progressive increase of ^{89}Zr-DFO-isatuximab uptake in bone and in bone marrow, which peaks at 120 h (23.6 ± 0.3 and 33.9 ± 21.2% ID/g). As expected, the highest uptake in blood pool and lungs was seen at the earliest time point, decreasing gradually (4.8 ±

https://doi.org/10.1021/acsomega.3c00624
ACS Omega 2023, 8, 22486−22495

0.3 and 6.1 ± 0.6%ID/g at 48 h, respectively), while uptake in liver remained relatively constant (18−10%ID/g).

Autoradiography Imaging and *Ex Vivo* Tissue Staining. Autoradiography imaging of select bones further demonstrated the specific uptake shown by the imaging data (Figure 5A). Finally, *ex vivo* flow cytometry analysis of extracted bone marrow cells confirmed the expression of CD38 (Figure 5B). Analogous data was obtained by immunohistochemistry staining of dissected femurs (Figures 5C and S3). CD38 expression was not detectable in healthy control femurs (Figure S4).

CD38-Targeted PET Imaging of ^{89}Zr-DFO-Isatuximab in a Disseminated Murine Model of Non-Hodgkin Lymphoma. To demonstrate that the use of ^{89}Zr-DFO-isatuximab as an immunoPET agent can be extended to other hematological malignancies, we conducted the same studies in a disseminated model of Burkitt's lymphoma, a very well-established model of CD38+ lymphoma. As shown by the PET/CT images (Figure 6A), uptake of ^{89}Zr-DFO-isatuximab by the tumor increases over time, displaying an exceptional contrast and delineation of the lymphoma lesions that matches the bioluminescence imaging. In fact, the contrast is almost superior to that obtained in the MM.1S-model, an outcome in accordance with the superior expression of the CD38 receptor, as consistenly determined by different *in vitro* evaluations. Regions of interest (ROI) on the corresponding PET images were used to determine the time-course tracer uptake by the organs of interest (Figure 6B). Slow clearance is observed from heart, lungs, and liver while a relatively constant uptake is observed for leg and lumbar spine, peaking at 120 h (15.4 ± 5.1 and 16.8 ± 3.1%ID/g, respectively).

DISCUSSION

Current measurements of MM disease burden—whether by blood analysis, imaging, or blind bone marrow biopsy—are suboptimal, greatly hampering clinical care.[8] For example, the limited sensitivity of standard 18F-FDG imaging for MM detection is well-recognized. Several studies have shown that at least 11% of patients are false negative on 18F-FDG due to the low hexokinase-2 expression,[33,34] and this false-negative rate can increase up to 60% in pretreated myeloma patients.[35] Thus, there exists an urgent need for the development of a superior, noninvasive PET imaging agent that can not only determine tumor burden but also predict the effectiveness of a selected therapy, monitor treatment response, and rule out MRD, improving the prognosis of patients. Ultimately, the use of such an agent could be extended to the targeted imaging and treatment of other hematologic malignancies such as lymphomas and leukemias.

We used isatuximab, the latest FDA-approved CD38-targeting antibody for MM treatment, for the synthesis and preclinical validation of (^{89}Zr)-labeled isatuximab as an immunoPET agent in one negative and two positive models of disease. We successfully demonstrated that ^{89}Zr-DFO-isatuximab is a highly selective and specific agent for MM imaging, capable of delivering results of equal quality to those previously obtained with ^{89}Zr-DFO-daratumumab—the reference in the literature for this malignancy in recent years.[12] Finally, we demonstrated ^{89}Zr-DFO-isatuximab's excellent imaging performance in a preclinal model of lymphoma, opening the door to further extending its application to this hematological malignancy.

The development and validation of this new radioagent could contribute greatly to MM research. Despite daratumumab's success both as an immunotherapy and immunoPET agent, acquired resistance is a recurrent problem among many MM patients. Introducing a substitute agent with a different mechanism of action may offer numerous patients a suitable therapeutic alternative. In fact, clinical trials are currently evaluating the value of isatuximab in daratumumab-refractory patients (NCT02514668). Thus, a matching imaging pair could contribute to the development of new and personalized diagnostic and treatment strategies.

More importantly, the faster tumor accumulation observed for ^{89}Zr-DFO-isatuximab and the fact that native isatuximab does not induce CD38 release from the cell surface, as daratumumab does, could allow for shorter imaging times via pretargeting strategies, reducing radiation exposure to patients and improving quality of life.

Overall, the high specificity and sensitivity of ^{89}Zr-DFO-isatuximab supports its clinical translation as a new imaging agent. As isatuximab is already an FDA-approved antibody, we expect this will ease and speed up the first-in-human clinical trial of the derived PET and future therapeutic agents.

CONCLUSION

The findings of this study suggest ^{89}Zr-DFO-isatuximab can be used as a noninvasive diagnostic PET agent to detect the presence of CD38-positive lesions, opening the door to an optimized and/or alternative agent for patients suffering from these malignancies that could improve their prognosis and survival.

ASSOCIATED CONTENT

Supporting Information

The Supporting Information is available free of charge at https://pubs.acs.org/doi/10.1021/acsomega.3c00624.

Detailed information on antibody characterization, *in vitro* binding assays, immunohistochemistry, flow cytometry, and biodistribution studies (PDF)

AUTHOR INFORMATION

Corresponding Author

Jason S. Lewis − *Department of Radiology and Program in Pharmacology, Memorial Sloan Kettering Cancer Center, New York, New York 10065, United States; Departments of Pharmacology and Radiology, Weill Cornell Medicine, New York, New York 10065, United States;* orcid.org/0000-0001-7065-4534; Email: lewisj2@mskcc.org

Authors

Natalia Herrero Alvarez − *Department of Radiology and Program in Pharmacology, Memorial Sloan Kettering Cancer Center, New York, New York 10065, United States*

Alexa L. Michel − *Department of Radiology and Program in Pharmacology, Memorial Sloan Kettering Cancer Center, New York, New York 10065, United States*

Tara D. Viray − *Department of Radiology and Program in Pharmacology, Memorial Sloan Kettering Cancer Center, New York, New York 10065, United States*

Marius E. Mayerhoefer − *Department of Radiology and Program in Pharmacology, Memorial Sloan Kettering Cancer Center, New York, New York 10065, United States*

Complete contact information is available at:

https://doi.org/10.1021/acsomega.3c00624
ACS Omega 2023, 8, 22486−22495

https://pubs.acs.org/10.1021/acsomega.3c00624

Author Contributions

Conception and design: N.H.A. and J.S.L. Development and methodology: N.H.A. and J.S.L. Acquisition of data: N.H.A., A.L.M., and T.D.V. Analysis and interpretation of data: N.H.A. Writing, review, and/or revision of the manuscript: N.H.A., M.E.M., and J.S.L. Study supervision: J.S.L.

Notes

The authors declare no competing financial interest.

■ ACKNOWLEDGMENTS

The authors would like to acknowledge the Radiochemistry and Molecular Imaging Probes Core Facility, the Small Animal Imaging Facility, and the Molecular Cytology Core Facility. The study was supported in part by R35 CA232130 (J.S.L.). The Radiochemistry and Molecular Imaging Probes Core Facility, the Small Animal Imaging Facility, and the Molecular Cytology Core Facility were supported in part by NIH P30 CA08748.

■ REFERENCES

(1) Siegel, R. L.; Miller, K. D.; Fuchs, H. E.; Jemal, A. Cancer statistics, 2022. *CA: A Cancer Journal for Clinicians* **2022**, *72* (1), 7−33.

(2) Kazandjian, D. Multiple myeloma epidemiology and survival: A unique malignancy. *Seminars in Oncology* **2016**, *43* (6), 676−681.

(3) Mateos, M. V.; Landgren, O. MGUS and Smoldering Multiple Myeloma: Diagnosis and Epidemiology. *Cancer Treat Res.* **2016**, *169*, 3−12.

(4) Mesguich, C.; Zanotti-Fregonara, P.; Hindié, E. New Perspectives Offered by Nuclear Medicine for the Imaging and Therapy of Multiple Myeloma. *Theranostics* **2016**, *6* (2), 287−90.

(5) Sachpekidis, C.; Goldschmidt, H.; Dimitrakopoulou-Strauss, A. Positron Emission Tomography (PET) Radiopharmaceuticals in Multiple Myeloma. *Molecules* **2020**, *25* (1), 134.

(6) Hogan, K. A.; Chini, C. C. S.; Chini, E. N. The Multi-faceted Ecto-enzyme CD38: Roles in Immunomodulation, Cancer, Aging, and Metabolic Diseases. *Frontiers in Immunology* **2019**, *10*, 1187.

(7) Chini, E. N.; Chini, C. C. S.; Espindola Netto, J. M.; de Oliveira, G. C.; van Schooten, W. The Pharmacology of CD38/NADase: An Emerging Target in Cancer and Diseases of Aging. *Trends Pharmacol. Sci.* **2018**, *39* (4), 424−436.

(8) Ulaner, G. A.; Landgren, C. O. Current and potential applications of positron emission tomography for multiple myeloma and plasma cell disorders. *Best Practice & Research Clinical Haematology* **2020**, *33* (1), 101148−101148.

(9) van de Donk, N. W. C. J.; Usmani, S. Z. CD38 antibodies in multiple myeloma: Mechanisms of action and modes of resistance. *Frontiers in Immunology* **2018**, *9* (SEP), 2134.

(10) Nooka, A. K.; Kaufman, J. L.; Hofmeister, C. C.; Joseph, N. S.; Heffner, T. L.; Gupta, V. A.; Sullivan, H. C.; Neish, A. S.; Dhodapkar, M. V.; Lonial, S. Daratumumab in multiple myeloma. *Cancer* **2019**, *125* (14), 2364−2382.

(11) Ghai, A.; Maji, D.; Cho, N.; Chanswangphuwana, C.; Rettig, M.; Shen, D.; DiPersio, J.; Akers, W.; Dehdashti, F.; Achilefu, S.; Vij, R.; Shokeen, M. Preclinical Development of CD38-Targeted [89Zr]Zr-DFO-Daratumumab for Imaging Multiple Myeloma. *J. Nucl. Med.* **2018**, *59* (2), 216−222.

(12) Ulaner, G. A.; Sobol, N. B.; O'Donoghue, J. A.; Kirov, A. S.; Riedl, C. C.; Min, R.; Smith, E.; Carter, L. M.; Lyashchenko, S. K.; Lewis, J. S.; Landgren, C. O. CD38-targeted Immuno-PET of Multiple Myeloma: From Xenograft Models to First-in-Human Imaging. *Radiology* **2020**, *295* (3), 606−615.

(13) Gouard, S.; Maurel, C.; Marionneau-Lambot, S.; Dansette, D.; Bailly, C.; Guérard, F.; Chouin, N.; Haddad, F.; Alliot, C.; Gaschet, J. Targeted-Alpha-Therapy Combining Astatine-211 and anti-CD138 Antibody in A Preclinical Syngeneic Mouse Model of Multiple Myeloma Minimal Residual Disease. *Cancers (Basel)* **2020**, *12* (9), 2721.

(14) Dawicki, W.; Allen, K. J. H.; Jiao, R.; Malo, M. E.; Helal, M.; Berger, M. S.; Ludwig, D. L.; Dadachova, E. Daratumumab-225Actinium conjugate demonstrates greatly enhanced antitumor activity against experimental multiple myeloma tumors. *OncoImmunology* **2019**, *8* (8), e1607673.

(15) Cho, N.; Ko, S.; Shokeen, M. Preclinical Development of Near-Infrared-Labeled CD38-Targeted Daratumumab for Optical Imaging of CD38 in Multiple Myeloma. *Mol. Imaging Biol.* **2021**, *23* (2), 186−195.

(16) Saltarella, I.; Desantis, V.; Melaccio, A.; Solimando, A. G.; Lamanuzzi, A.; Ria, R.; Storlazzi, C. T.; Mariggiò, M. A.; Vacca, A.; Frassanito, M. A. Mechanisms of Resistance to Anti-CD38 Daratumumab in Multiple Myeloma. *Cells* **2020**, *9* (1), 167.

(17) Kambhampati, S.; Wen, K. W.; Sung, V.; Wong, S. W. K.; Martin, T. G.; Wolf, J. L.; Shah, N.; Wiita, A. Investigating macrophage function as a mechanism of resistance to daratumumab in relapsed refractory multiple myeloma patients. *Journal of Clinical Oncology* **2020**, *38*, No. e20547.

(18) Chillemi, A.; Zaccarello, G.; Quarona, V.; Ferracin, M.; Ghimenti, C.; Massaia, M.; Horenstein, A. L.; Malavasi, F. Anti-CD38 antibody therapy: windows of opportunity yielded by the functional characteristics of the target molecule. *Mol. Med.* **2013**, *19* (1), 99−108.

(19) Krejcik, J.; Casneuf, T.; Nijhof, I. S.; Verbist, B.; Bald, J.; Plesner, T.; Syed, K.; Liu, K.; van de Donk, N. W.; Weiss, B. M.; et al. Daratumumab depletes CD38+ immune regulatory cells, promotes T-cell expansion, and skews T-cell repertoire in multiple myeloma. *Blood* **2016**, *128* (3), 384−94.

(20) Neri, P.; Maity, R.; Tagoug, I.; Duggan, P.; McCulloch, S.; Jimenez-Zepeda, V.; Tay, J.; Boise, L. H.; Thakurta, A.; Bahlis, N. J. Single Cell Resolution Profiling Defines the Innate and Adaptive Immune Repertoires Modulated By Daratumumab and IMiDs Treatment in Multiple Myeloma (MM). *Blood* **2017**, *130*, 123.

(21) Nijhof, I. S.; Casneuf, T.; van Velzen, J.; van Kessel, B.; Axel, A. E.; Syed, K.; Groen, R. W.; van Duin, M.; Sonneveld, P.; Minnema, M. C.; et al. CD38 expression and complement inhibitors affect response and resistance to daratumumab therapy in myeloma. *Blood* **2016**, *128* (7), 959−70.

(22) Usmani, S. Z.; Karanes, C.; Bensinger, W. I.; D'Souza, A.; Raje, N.; Tuchman, S. A.; Sborov, D.; Laubach, J. P.; Bianchi, G.; Kanagavel, D.; et al. Final results of a phase 1b study of isatuximab short-duration fixed-volume infusion combination therapy for relapsed/refractory multiple myeloma. *Leukemia* **2021**, *35* (12), 3526−3533.

(23) Mikhael, J.; Belhadj-Merzoug, K.; Hulin, C.; Vincent, L.; Moreau, P.; Gasparetto, C.; Pour, L.; Spicka, I.; Vij, R.; Zonder, J.; et al. A phase 2 study of isatuximab monotherapy in patients with multiple myeloma who are refractory to daratumumab. *Blood Cancer J.* **2021**, *11* (5), 89.

(24) Deckert, J.; Wetzel, M.-C.; Bartle, L. M.; Skaletskaya, A.; Goldmacher, V. S.; Vallée, F.; Zhou-Liu, Q.; Ferrari, P.; Pouzieux, S.; Lahoute, C.; et al. SAR650984, A Novel Humanized CD38-Targeting Antibody, Demonstrates Potent Antitumor Activity in Models of Multiple Myeloma and Other CD38^{+} Hematologic Malignancies. *Clin. Cancer Res.* **2014**, *20* (17), 4574−4583.

(25) Martin, T. G.; Corzo, K.; Chiron, M.; van de Velde, H.; Abbadessa, G.; Campana, F.; Solanki, M.; Meng, R.; Lee, H.; Wiederschain, D.; et al. Therapeutic Opportunities with Pharmacological Inhibition of CD38 with Isatuximab. *Cells* **2019**, *8* (12), 1522.

(26) Kinder, M.; Bahlis, N. J.; Malavasi, F.; De Goeij, B.; Babich, A.; Sendecki, J.; Rusbuldt, J.; Bellew, K.; Kane, C.; Van de Donk, N. Comparison of CD38 antibodies in vitro and ex vivo mechanisms of action in multiple myeloma. *Haematologica* **2021**, *106* (7), 2004−2008.

(27) Lee, H. T.; Kim, Y.; Park, U. B.; Jeong, T. J.; Lee, S. H.; Heo, Y.-S. Crystal structure of CD38 in complex with daratumumab, a first-in-class anti-CD38 antibody drug for treating multiple myeloma. *Biochem. Biophys. Res. Commun.* **2021**, *536*, 26−31.
(28) Mikhael, J.; Belhadj-Merzoug, K.; Hulin, C.; Vincent, L.; Moreau, P.; Gasparetto, C.; Pour, L.; Spicka, I.; Vij, R.; Zonder, J.; et al. A phase 2 study of isatuximab monotherapy in patients with multiple myeloma who are refractory to daratumumab. *Blood Cancer Journal* **2021**, *11* (5), 89.
(29) Moreno, L.; Perez, C.; Zabaleta, A.; Manrique, I.; Alignani, D.; Ajona, D.; Blanco, L.; Lasa, M.; Maiso, P.; Rodriguez, I.; et al. The Mechanism of Action of the Anti-CD38 Monoclonal Antibody Isatuximab in Multiple Myeloma. *Clin. Cancer Res.* **2019**, *25* (10), 3176−3187.
(30) Richardson, P. G.; Beksaç, M.; Špička, I.; Mikhael, J. Isatuximab for the treatment of relapsed/refractory multiple myeloma. *Expert Opin Biol. Ther* **2020**, *20* (12), 1395−1404.
(31) Richardson, P. G.; Harrison, S. J.; Bringhen, S.; Schjesvold, F.; Yong, K.; Campana, F.; Le-Guennec, S.; Macé, S.; Dimopoulos, M. A. Isatuximab for relapsed/refractory multiple myeloma: review of key subgroup analyses from the Phase III ICARIA-MM study. *Future Oncology* **2021**, *17* (34), 4797−4812.
(32) Sharma, S. K.; Lyashchenko, S. K.; Park, H. A.; Pillarsetty, N.; Roux, Y.; Wu, J.; Poty, S.; Tully, K. M.; Poirier, J. T.; Lewis, J. S. A rapid bead-based radioligand binding assay for the determination of target-binding fraction and quality control of radiopharmaceuticals. *Nucl. Med. Biol.* **2019**, *71*, 32−38.
(33) Rasche, L.; Angtuaco, E.; McDonald, J. E.; Buros, A.; Stein, C.; Pawlyn, C.; Thanendrarajan, S.; Schinke, C.; Samant, R.; Yaccoby, S.; et al. Low expression of hexokinase-2 is associated with false-negative FDG-positron emission tomography in multiple myeloma. *Blood* **2017**, *130* (1), 30−34.
(34) Abe, Y.; Ikeda, S.; Kitadate, A.; Narita, K.; Kobayashi, H.; Miura, D.; Takeuchi, M.; O'Uchi, E.; O'Uchi, T.; Matsue, K. Low hexokinase-2 expression-associated false-negative (18)F-FDG PET/CT as a potential prognostic predictor in patients with multiple myeloma. *Eur. J. Nucl. Med. Mol. Imaging* **2019**, *46* (6), 1345−1350.
(35) Kircher, S.; Stolzenburg, A.; Kortüm, K. M.; Kircher, M.; Da Via, M.; Samnick, S.; Buck, A. K.; Einsele, H.; Rosenwald, A.; Lapa, C. Hexokinase-2 Expression in (11)C-Methionine-Positive, (18)F-FDG-Negative Multiple Myeloma. *J. Nucl. Med.* **2019**, *60* (3), 348−352.

https://doi.org/10.1021/acsomega.3c00624
ACS Omega 2023, 8, 22486−22495